Electrochimica Acta 299 (2019) 727–735

Contents lists available at ScienceDirect

Electrochimica Acta

journal homepage: www.elsevier.com/locate/electacta

Comparison of faradaic reactions in flow-through and flow-by capacitive deionization (CDI) systems

Changyong Zhang [a], Di He [b, c], Jinxing Ma [a], Wangwang Tang [d, e], T. David Waite [a, *]

[a] School of Civil and Environmental Engineering, University of New South Wales, Sydney, NSW 2052, Australia
[b] Institute of Environmental Health and Pollution Control, Guangdong University of Technology, Guangzhou, 510006, China
[c] Guangzhou Key Laboratory of Environmental Catalysis and Pollution Control, School of Environmental Science and Engineering, University of Technology, Guangzhou, 510006, China
[d] College of Environmental Science and Engineering, Hunan University, Changsha, 410082, China
[e] Key Laboratory of Environmental Biology and Pollution Control, Ministry of Education, Hunan University, Changsha, 410082, China

ARTICLE INFO

Article history:
Received 16 October 2018
Received in revised form
16 December 2018
Accepted 10 January 2019
Available online 11 January 2019

Keywords:
Flow-through CDI
Faradaic reactions
pH fluctuation
Forward flow
Reverse flow

ABSTRACT

Use of flow-through electrodes, in which water flows through rather than past porous electrodes, has been shown to be a promising approach to overcoming mass transfer limitations in various electrochemical technologies (including microbial fuel cells, electrochemical disinfection, electrochemical advanced oxidation processes and capacitive deionization). In this work, we fabricated a flow-through CDI cell and investigated the saline water desalination performance and the possible Faradaic reactions occurring in the systems under different flow modes, *i.e.*, forward mode (water flows from anode to cathode) and reverse flow mode (water flows from cathode to anode). Upon applying a charging voltage of 1.2 V, use of flow-through CDI operating under both flow conditions exhibited better desalination performance compared to that of conventional flow-by CDI. Larger pH fluctuations were found in flow-through CDI systems with effluent pH increasing to about 9.3 in forward flow mode and decreasing to 3.8 under reverse flow mode while in flow-by CDI, the treated water pH exhibited only a slight increase to 8.0. In addition, much higher H_2O_2 production and dissolved oxygen (DO) decay rates were observed in flow-through CDI operated in forward flow mode compared to other scenarios, possibly due to the different ion adsorption and reaction sequences. These findings provide insight into both the desalination capacity of flow-through CDI and the Faradaic reactions occurring in such a system and should be of value in developing a treatment technology capable of simultaneous water desalination, disinfection and/or micro-pollutant removal.

1. Introduction

The requirement for sufficient fresh potable water is generally acknowledged as one of the most critical issues of the 21st century [1]. Recently, renewed attention has been given to capacitive deionization (CDI) in view of the potential for brackish water desalination with greater energy efficiency and cost-effectiveness compared to conventional desalination technologies such as reverse osmosis (RO), electrodialysis (ED) and multistage flash distillation (MSF) [1,2]. The basic principle of CDI involves the application of a potential difference to a pair of porous (typically carbon) electrodes such that ions in the solution are removed and immobilized in the electrical double-layer (EDL) of the oppositely charged electrode. When the potential is either removed or reversed, the adsorbed ions are released to bulk solution and the electrodes regenerated [2].

Over the past decade, more than a dozen different CDI cell architectures including flow-by CDI, flow-through CDI, membrane CDI, flow electrode CDI and inverted CDI have been developed with the purpose of optimizing salt adsorption capacity, energy efficiency and electrode regeneration rate [2–7]. However, the earliest and most widely-used architecture is flow-by CDI in which water flows adjacent to electrode pairs that are separated from each other by a spacer. While easier to assemble and seal than alternate designs, this classical architecture suffers from several limitations

---

* Corresponding author.

E-mail addresses: changyong.zhang@unsw.edu.au (C. Zhang), di.he@gdut.edu.cn (D. He), jinxing.ma@unsw.edu.au (J. Ma), tangwangwang89@gmail.com (W. Tang), d.waite@unsw.edu.au (T.D. Waite).

https://doi.org/10.1016/j.electacta.2019.01.058

including (i) long spacer-to-electrode diffusion times, (ii) high cell internal resistance and volume due to the need for a relatively thick separator between the electrodes, and (iii) insufficient utilization of the adsorption capacity of the porous carbon electrodes [8,9]. Of the alternatives available, flow-through architecture, in which water flows directly from one electrode to another, has been found to be a promising configuration because of the enhanced contact time and mass transfer. Flow-through technologies have been applied in a number of electrochemical water treatment processes including electrochemical membrane filtration [10–12], electrochemical disinfection [13,14], energy production using microbial fuel cells [15,16] and capacitive desalination [9,17]. Flow-through CDI was first proposed by Newman and Johnson [18,19] and further developed by Suss et al. [9]. In the configuration used by these investigators, the feed water flows straight through the macropores of the electrodes along the primary electric field direction with this configuration resulting in enhanced mass transfer of ions to the micropores with a higher desalting performance and charge efficiency compared to the typical flow-by configuration [9,20].

Both non-Faradaic and Faradaic reactions occur in CDI systems with non-Faradaic reactions involving the storage of ions in the EDL at the carbon/electrolyte interface upon charging recognized to be the primary mechanism of desalination [1,21]. Faradaic reactions however are also recognized to be important to the performance of CDI [21–24]. At the anode (*i.e.*, the electrode that is positively charged during electrosorption), oxidation reactions including carbon electrode oxidation, water oxidation and, potentially, chloride oxidation [22,25] may occur while reduction reactions such as oxygen reduction take place at the cathode (*i.e.*, the electrode that is negatively charged during electrosorption) [22,26]. On one hand, these reactions lead to a series of unexpected side effects such as deterioration in desalination efficiency, decrease in electrode lifespan, precipitation on membrane surface or pores, increase in energy consumption, formation of by-products and fluctuation of the effluent water quality [1,27–29]. On the other hand, the *in-situ* generated reactive species such as H_2O_2 and HOCl, if managed properly, can enable CDI to fulfil its promise of multifunctionality such as micropollutant degradation and/or water disinfection [22].

Comprehensive understanding of the Faradaic reactions occurring in CDI systems is vital if CDI is to be operated in a stable manner for long periods and with optimal energy consumption. In our previous work, we have investigated the Faradaic reactions in flow-by CDI [22], membrane CDI [30] and flow electrode CDI [31–34] and, recently, published a review paper on Faradaic reactions in CDI [21]. However, there has been limited investigation of Faradaic processes in CDI systems based on flow-through architecture. As the feedwater is forced to flow directly from one electrode to the other, ion transfer may be expected to differ from that in conventional flow-by CDI, potentially enhancing the rate and extent of Faradaic reactions that occur. As such, the desalination performance and Faradaic reactions in flow-through CDI systems operating under different water flow modes (*i.e.*, forward and reverse flow) are investigated in this study with variation of solution pH and dissolved oxygen (DO) and the production of H_2O_2 examined. A comprehensive discussion of the side effects and the potential benefits of the Faradaic reactions occurring in these flow-through systems is provided at the end of this work.

2. Materials and methods

2.1. Cell design

The CDI cell (Fig. S1) used in this study consisted of two parallel commercial carbon cloth electrodes (Nantong Senyou Carbon Fiber Co., Nantong, China) with a macroscopic dimension of $4.0 \times 4.0 \times 0.3\ \text{cm}^3$ (Fig. S2). The surface area of carbon cloth electrode measured by Brunauer-Emmett-Teller (BET) method was $1101\ \text{m}^2\ \text{g}^{-1}$ as reported in our previous work [30]. Graphite sheets were attached to the carbon cloth electrodes and served as the current collectors.

For the flow-through CDI cell, laser cut silicone gaskets of dimension $4.0 \times 4.0 \times 0.2\ \text{cm}^3$ served as upstream and downstream reservoirs permitting the feedwater to pass evenly through the electrodes and separator. A layer of porous nonconductive nylon sheet (100-mesh, $55\ \text{mm} \times 55\ \text{mm} \times 0.2\ \text{mm}$) was used to electronically isolate the electrodes (Fig. 1). Two operational modes (*i.e.*,

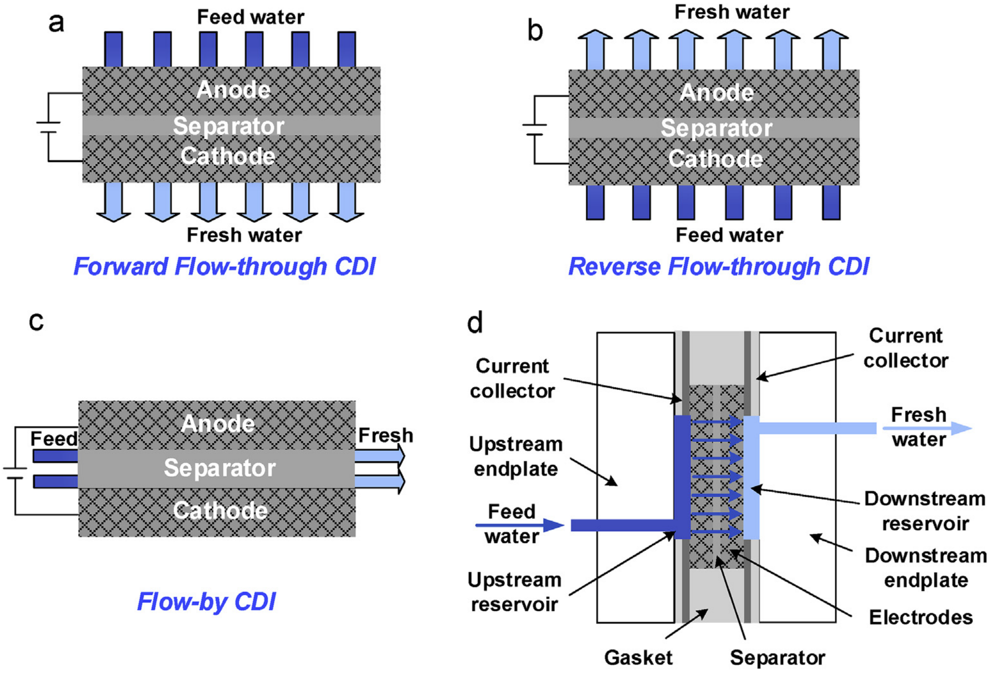

Fig. 1. Schematic of CDI cell configuration, (a) forward flow-through CDI, (b) reverse flow-through CDI, (c) flow-by CDI, (d) the cross-section of the flow-through CDI cell.

forward and reverse flow) were investigated in the flow-through CDI (Fig. 1a and b). In the forward flow-through scenario, the feedwater first passed through the anode, followed by the separator and, finally, the cathode (Fig. 1a). In reverse flow-through scenario, the feedwater flowed in an opposite direction (Fig. 1b). For comparison, a flow-by CDI cell was also fabricated without the use of upstream and downstream reservoirs due the fact that feedwater flows in the separator channel, in parallel with the electrodes (Fig. 1c). In order to prevent the short-circuiting between the two electrodes and provide unobstructed flow pathway for the feed water, two layers of separator is used in flow-by CDI cell. A cross-section view of the flow-through CDI is shown in Fig. 1d.

2.2. Experimental setup

In all desalination experiments, a feed solution containing 5 mM sodium chloride with an initial DO concentration of 6.5 mg L^{-1} was pumped from the recycling container, passed through the CDI cell, and then returned to the recycling container (Fig. 2). The solution flow rate (0.78 mL s^{-1}) was controlled by a peristaltic pump (Masterflex, Cole-Parmer, USA). The solution conductivity, pH, and DO were monitored using an electrical conductivity (EC) meter (F-54, HORIBA, Japan), a pH meter (F-51, HORIBA, Japan), and a DO probe (DO-BTA, Vernier Corp.), respectively (Fig. S1) [35]. The cell potential, measured by a digital multimeter (Jaycar Electronics, Australia), was set to 0 V prior to the desalination test. During each charging stage, a constant potential was applied between the anode and the cathode for 15 min using a DC power supply. During the discharging step, the CDI electrodes were short-circuited for 15 min. Prior to each test, the CDI cell was fully flushed using Milli-Q water.

2.3. Analytical methods

The salt adsorption capacity (*SAC*) was calculated according to the equation:

$$\mathrm{SAC} = \frac{(C_0 - C_t) \times V_s}{m} \tag{1}$$

where C_0 and C_t are the salt concentrations (mg L^{-1}) at the beginning of the experiment and at time *t*, respectively. V_s is the volume of feedwater (100 mL) used in this work and *m* is the total mass of the two carbon electrodes (g).

The charge efficiency (η_{charge}) can be calculated as follows:

$$\eta_{\mathrm{charge}} = \frac{n \times (C_0 - C_t) \times V_s \times F}{M \times \int idt} \times 100\% \tag{2}$$

where n_{charge} represents the number of electrons needed for the removal of 1 mol of NaCl, V_s is the volume of feed water (100 mL), *F* represents the Faraday constant (96,485 C mol^{-1}), *M* is the

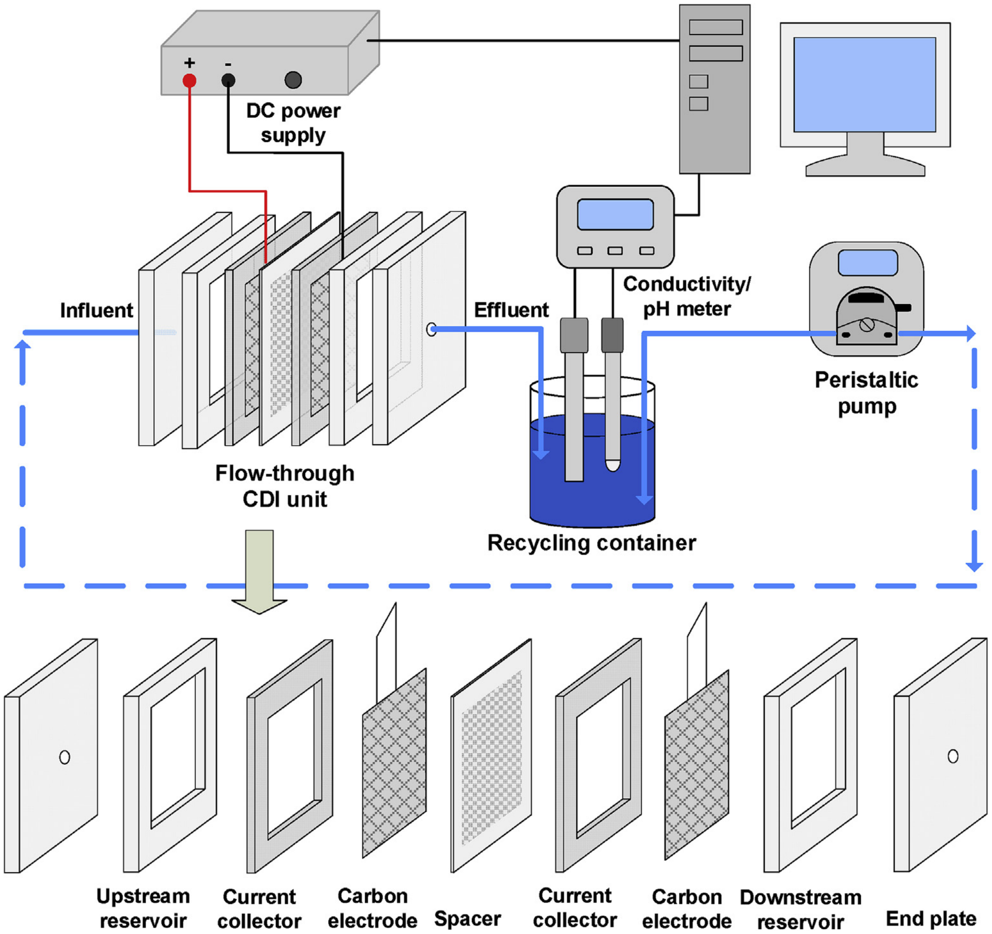

Fig. 2. Schematic of the flow-through CDI cell setup. Two pieces of carbon cloth served as anode and cathode and a DC power source used to provide a constant voltage (1.2 V). Conductivity and pH sensors were used to detect the solution conductivity and pH in the recycling container.

molecular weight of sodium chloride (58.5 g mol^{-1}) and i represents the current at time t (A). Note that $t = 0$ was defined as the time point when the electrical adsorption was initiated.

The concentration of H_2O_2 was determined using the Amplex Red (AR)/horseradish peroxidase (HRP) method [36]. Specially, samples were diluted with 10 mM MOPs buffer (pH 7.0–7.1) and mixed with AR/HRP stock solution in which AR is oxidized by H_2O_2 in the presence of horseradish peroxidase (HRP), exhibiting a fluorescence emission maxima at 587 nm upon excitation at 563 nm, allowing the quantification of H_2O_2 in the solution.

3. Results and discussion

3.1. CDI performance

Fig. 3a–c shows the temporal variation of conductivity of the desalinated water in flow-through and flow-by CDI systems. Obviously, it can be observed that salt was removed more effectively in flow-through CDI mode compared to flow-by CDI mode in all scenarios. For instance, when a potential difference of 1.2 V was applied, the feedwater conductivity first decreased sharply and then reached a relatively steady concentration within 15 min. Flow-through CDI operated in forward flow mode achieved the highest salt adsorption capacity (11.1 mg g^{-1}), which is 36.3% and 24.3% higher than that of flow-by CDI (8.2 mg g^{-1}) and flow-through CDI operated in reverse flow mode (10.2 mg g^{-1}). In addition to greatest overall salt removal in the forward flow-through mode, higher current and charge efficiency (53.6%) was also observed in flow-through CDI operated under forward flow mode (Fig. S3 and Fig. 3d).

In flow-through CDI setup, the fluid flows directly through the two electrodes with the result that the micropore spaces become more accessible to the ions, likely leading to the full use of the active sites of the carbon electrodes and improved salt removal performance [9,37]. In comparison, the relatively poor performance in flow-by mode might be due to the fact that the feedwater only flows between anode and cathode, which restricts the ion transport from the bulk solution into the inner parts of the electrodes, resulting in insufficient utilization of the adsorption capability of the carbon electrodes and associated low charge efficiency (Fig. 3b). In flow-by CDI, ions that have been initially adsorbed near the surface sites might act as barriers for further ion diffusion into the deeper sites. Meanwhile, thicker separator in the flow-by system also slightly increased cell internal resistance, therefore, lowering the salt adsorption capacity. It should also be noted that forward flow operation of flow-through CDI resulted in better desalting performance and higher charge efficiency than that achieved in reverse flow mode. Consideration was therefore given to characterising the competing Faradaic electron transfer reactions occurring during the deionization process.

3.2. Variation of pH

Variations of pH of the desalted water in flow-through and flow-by CDI systems are shown in Fig. 4a–c with the results revealing that the pH of the desalted water in flow-through CDI cell fluctuated more severely than in the case of flow-by CDI. For example, under a constant voltage of 1.2 V, pH increased to a peak value of 9.3

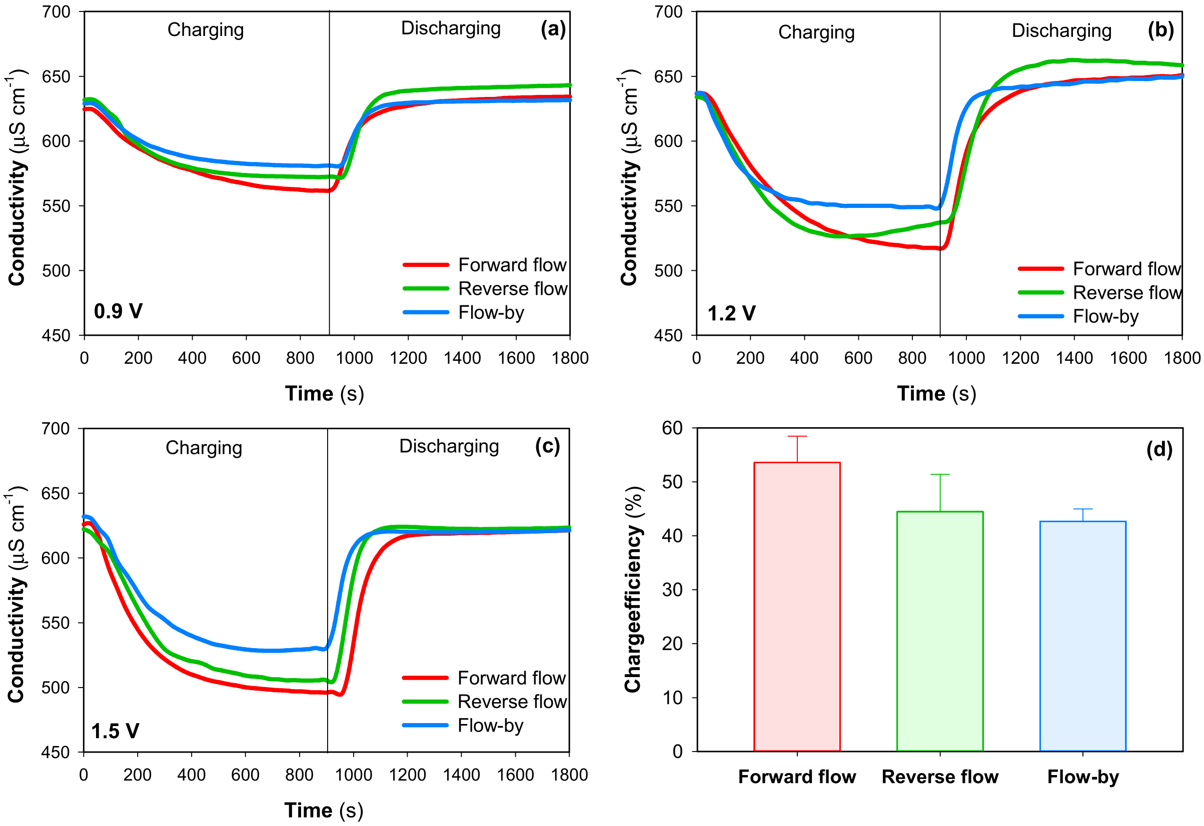

Fig. 3. Comparison of the temporal variation of conductivity at a constant potential of (a) 0.9 V, (b) 1.2 V, (c) 1.5 V in different scenarios (*i.e.*, flow-through CDI operated in forward flow mode, flow-through CDI operated in reverse flow mode and flow-by CDI); (d) comparison of the charge efficiency in different scenarios under a constant voltage of 1.2 V. Experimental conditions: 900 s charging at a constant potential followed by 900 s discharging by short-circulating the two electrodes.

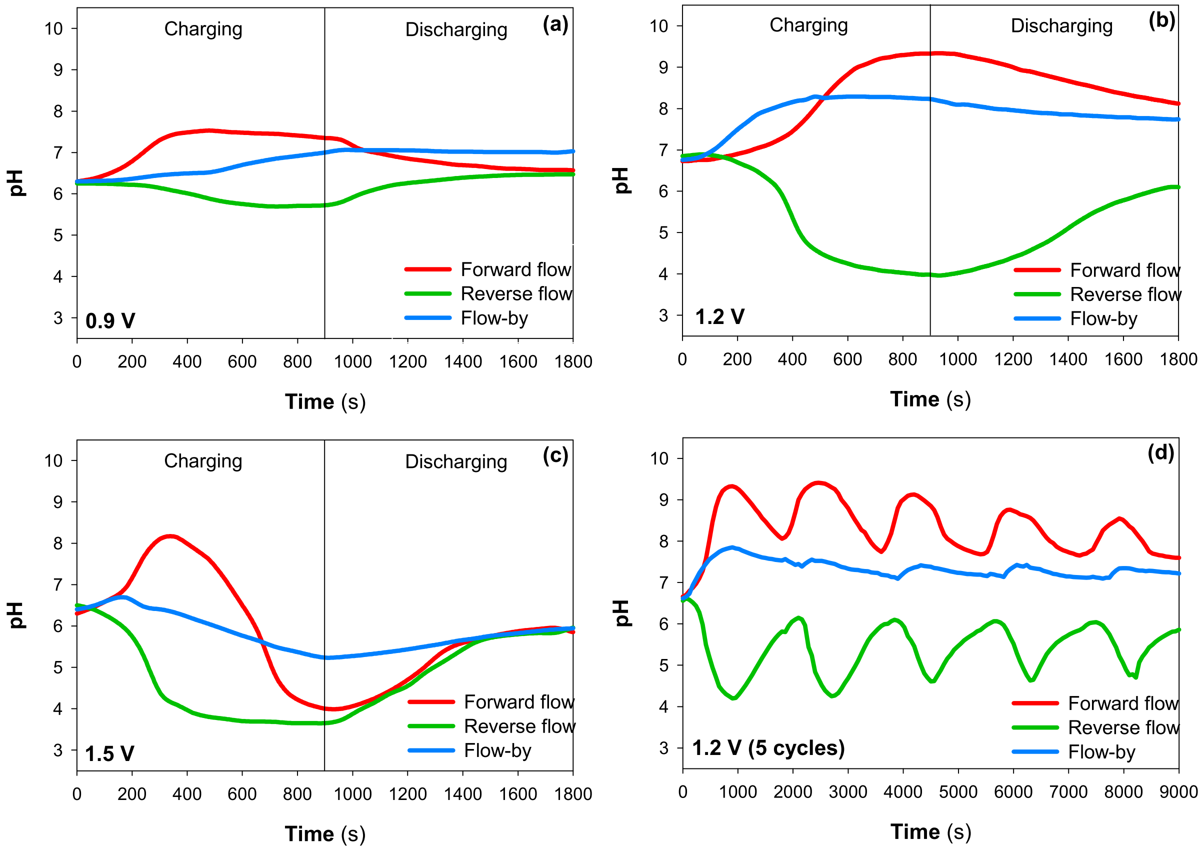

Fig. 4. Comparison of the temporal variation of pH at a constant potential of (a) 0.9 V, (b) 1.2 V, (c) 1.5 V in different scenarios (*i.e.*, flow-through CDI operated in forward flow mode, flow-through CDI operated in reverse flow mode and flow-by CDI); (d) pH variation when operating the system for 5 cycles under a constant voltage of 1.2 V. Experimental conditions: 900 s charging at a constant potential followed by 900 s discharging by short-circulating the two electrodes.

during the charging step and then decreased back to ~8.0 in the discharging step in a flow-through CDI operated in forward flow mode. When operated in reverse flow mode, the pH of the CDI effluent changed in a totally different manner with the pH decreasing to 3.8 in the charging stage followed by a gradual increase to ~6.0 in the discharging stage. In flow-by CDI mode, pH increased slightly (to about 8.2) and then remained relatively stable (Fig. 4b). Fig. 4d demonstrated that pH fluctuation extend gradually decreased during prolonged operation.

It has been reported that the pH fluctuations in CDI cells can be induced by both Faradaic and non-Faradaic processes [1]. Specifically, non-Faradaic processes including the selective electrosorption of H^+ and OH^- and asymmetric removal of anions and cations into the EDLs likely lead to imbalance of H^+/OH^- and pH variation. In a flow-through CDI system, as one ion is preferentially captured in the first electrodes (*e.g.*, Cl^- first being stored by the anode in forward flow mode), water dissociation occurs in the opposite electrode in order to maintain electroneutrality with these processes contributing to pH fluctuation (*i.e.*, pH increase in forward flow mode). Different ions in solution have different diffusion coefficients (mobilities), leading to a difference in ion movement and adsorption rate with the result that pH fluctuations occur. For instance, the diffusion coefficient of H^+ ($9.13 \times 10^{-9}\ m^2\ s^{-1}$) is significantly larger than that of OH^- ($5.16 \times 10^{-9}\ m^2\ s^{-1}$) suggesting that H^+ will be more mobile and be adsorbed at a faster rate than OH^- with this effect potentially contributing to the initial pH rise.

Faradic reactions, which consume/generate H^+/OH^- during the desalination process, have been recognized to be major contributors to effluent pH fluctuation. For example, anodic Faradaic reactions associated with the oxidation of carbon electrodes (and/or chloride and water) will take place during the desalination process resulting in the generation of H^+ (Eqs (3)–(8)). Additionally, cathodic Faradaic reactions, particularly those involving oxygen reductions, tend to consume H^+ and generate peroxide or water (Eqs (9)–(11)). Possible Faradaic reactions are summarized below:

Anodic oxidation reactions

$$\frac{1}{2}C+\frac{1}{2}H_2O\rightarrow\frac{1}{2}C=O_{ad}+H^++e^-\quad E^0=0.21\ V/SHE \tag{3}$$

$$\frac{1}{4}C+\frac{1}{2}H_2O\rightarrow\frac{1}{4}CO_2+H^++e^-\quad E^0=0.21\ V/SHE \tag{4}$$

$$\frac{1}{2}H_2O_2\rightarrow\frac{1}{2}O_2+H^++e^-\quad E^0=0.69\ V/SHE \tag{5}$$

$$Cl^-\rightarrow\frac{1}{2}Cl_2+e^-\quad E^0=1.36\ V/SHE \tag*{(5)}$$

$$Cl_2+H_2O\rightarrow HClO+H^++Cl^- \tag{7}$$

Cathodic reduction reactions

$$\frac{1}{2}O_2 + H^+ + e^- \rightarrow \frac{1}{2}H_2O_2 \quad E^0 = 0.69V/SHE \tag{8}$$

$$\frac{1}{2}H_2O_2 + H^+ + e^- \rightarrow H_2O \quad E^0 = 1.78V/SHE \tag{9}$$

$$C + H_2O + e^- \rightarrow C - H + OH^- \tag{10}$$

The more extreme pH fluctuations observed in flow-through CDI mode compared to flow-by CDI mode are expected as a result of the more abundant reaction sites and faster mass transfer rate (especially of oxygen) to the electrode surface in the flow-through case. Note that when flow-through CDI is operated in forward-flow mode, feedwater first passes through the anode and then the cathode with the result that the anodic Faradaic reactions (Eqs (3)–(7)) will occur first and generate extra H^+ which, subsequently, will be involved in the oxygen reactions (Eqs (8)–(10)) and consumed rapidly at the cathode. Therefore, after the feedwater flows out of the cell (post-cathode), the solution become alkaline reaching a pH value (9.3) higher than that observed in the flow-by system (8.0). In the reverse-flow case, feedwater first enters the cathode, where there are less H^+ to support the oxygen reduction reactions. Subsequently, the feed stream enters the anode, where carbon oxidation occurs with concomitant H^+ production and associated pH decrease (to 3.8). Meanwhile, the decomposition of H_2O_2 (transported from the cathode) at the anode (the reverse of the reaction shown in Eq (8)) could also contribute to H^+ formation and pH decrease. In the flow-by system, oxygen reduction reactions would be expected to be dominant compared to carbon oxidation reactions under an applied voltage of 1.2 V, which means that more H^+ will be consumed than generated, leading to an increase in effluent pH. However, since the Faradaic reactions are kinetically limited in flow-by mode, the extent of pH fluctuation is less significant than that of flow-through mode.

3.3. H_2O_2 production and DO decay

The oxygen reduction activity of the carbon cloth was examined by CV in N_2 and O_2 saturated NaCl solutions. As shown in Fig. S4, a reduction peak appeared when using O_2-saturated electrolyte, whereas a featureless curve was observed within the same voltage window in the N_2-saturated electrolyte with these results indicating that oxygen reduction occurred at the carbon electrode. The profiles of H_2O_2 concentration versus time during charging and discharging in the three scenarios are presented in Fig. 5a. It can be observed that H_2O_2 concentration increased rapidly at the start of the charging step but then gradually decreased in both flow-through CDI operated in forward flow mode and flow-by CDI, with the maximum H_2O_2 concentration reaching 45 and 37.5 μM, respectively. In reverse flow-through mode, H_2O_2 concentration exhibited a relatively slower increase and achieved a peak value of 17.6 μM at the end of the charging step. The charge consumed for H_2O_2 production accounted for 4.7%, 1.8% and 4.2% of the total charge applied for forward flow, reverse flow and flow-by system, respectively.

The production of H_2O_2 is expected to be accompanied by a decrease in DO concentration. Fig. 5b presents the temporal variation of DO concentration during charging and discharging cycles in the three scenarios. As expected, DO decreases rapidly in all cases during the charging period. The forward flow-through CDI system showed the largest rate of DO decay, with the DO concentration declining from 6.5 to 3.1 mg L^{-1}, while the least DO consumption (6.5–4.2 mg L^{-1}) was observed in reverse flow mode. In contrast, the DO decrease rate in the flow-by CDI system was between the flow-through cases.

In flow-through CDI operated in forward flow mode, H^+ generated from anodic Faradaic reactions will pass directly into the cathode, altering the local feedwater composition and contributing to sequential cathodic Faradaic reactions (Fig. 6). In accord with this, relatively rapid H_2O_2 production and DO consumption are observed in forward flow mode. However, in reverse flow mode, the solution first enters the cathode, where oxygen reduction and H_2O_2 formation reactions are expected to occur first (Fig. 6). With this flow pattern, the local H^+ concentration in the cathode will be much lower than is the case in forward flow mode and, as such, the oxygen reduction reaction will, therefore, be somewhat supressed. In addition, once the feedwater passes into the anode, the H_2O_2 formed at cathode will be further decomposed into water. All these factors presumably contribute to the lower H_2O_2 generation rate and DO decay rate observed in the reverse flow scenario than in the forward flow case. In the flow-by CDI case, the Faradaic reactions are less significant than in the forward flow configuration as they are constrained by the mass diffusion rate and limited reaction sites.

3.4. Electrode potentials

To further investigate the occurrence of these Faradaic reactions, the variations of both anode and cathode potentials were measured

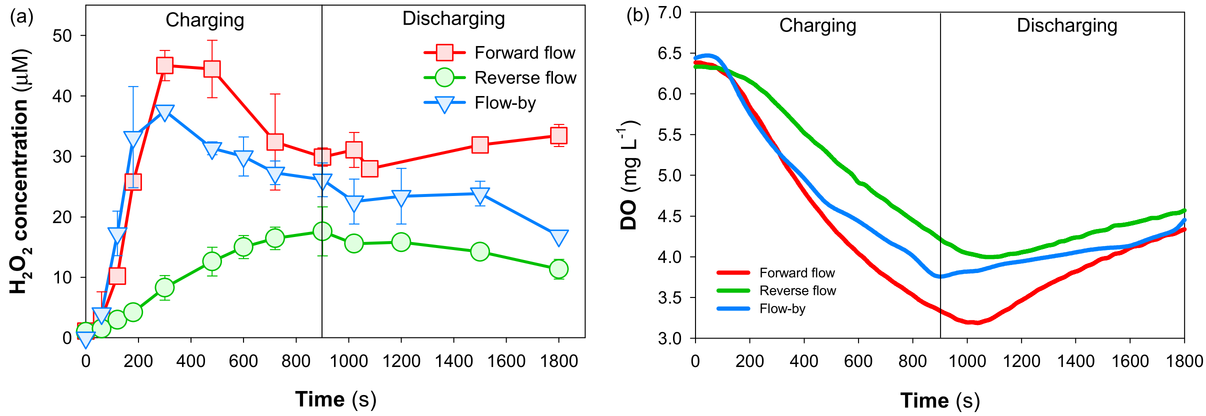

Fig. 5. Comparison of the temporal variations of (a) H_2O_2 and (b) DO in different scenarios (*i.e.*, flow-through CDI operated in forward flow mode, flow-through CDI operated in reverse flow mode, and flow-by CDI). Experimental conditions: 900 s charging at a constant potential of 1.2 V and 900 s discharging by short-circulating the two electrodes.

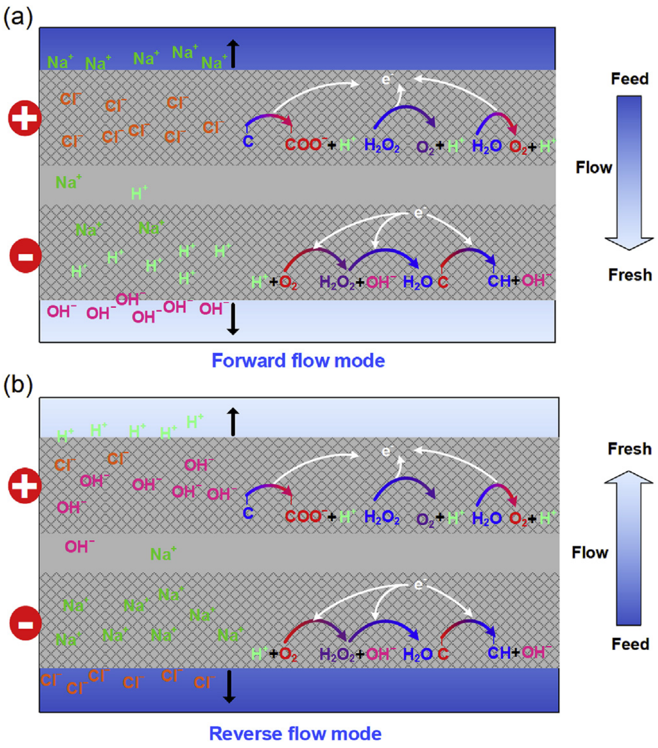

Fig. 6. Schematic diagram about the capacitive ion storage process and Faradaic reaction processes in flow-through system which operated in (a) forward flow mode, (b) reverse flow mode. Ions are preferentially electroadsorbed and Faradaic reactions are sequentially occurred depending on the flow direction resulting in the pH variation in the system. The black arrows indicate the electrode repulsion of ions with the same charge.

using an *in situ* inserted Ag/AgCl reference electrode. As presented in Fig. 7, asymmetric distributions of applied potential were observed in the CDI system. Both the anode and cathode potentials were around 0.3 V/SHE prior to the operation, however, on commencement of charging, the anode potentials immediately increased to about 0.8 V while the cathode potentials dropped to −0.4~-0.3 V in all scenarios. Interestingly, the potentials (both anode and cathode) of the forward flow mode were slightly lower than other operational modes, favouring the occurrence of cathodic Faradaic reactions (*i.e.,* oxygen reduction) and supressing the anodic Faradaic reactions (*i.e.,* carbon oxidation). The lower cathode potential would also enhance cation adsorption onto the lower-efficiency cathode, therefore, leading to better salt removal performance. As for the reverse flow mode, higher potentials (anode: ~1.0 V/SHE, cathode: −0.2 V/SHE) were observed during the charging periods, which could result in more severe anodic carbon oxidation and lower effluent pH.

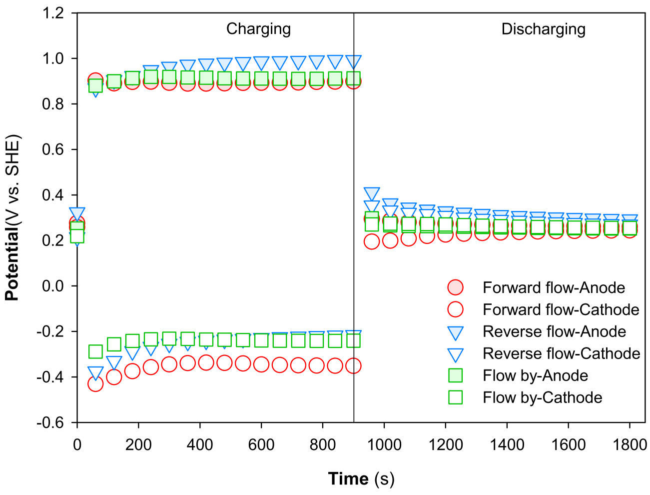

Fig. 7. Variation of the measured anode and cathode potential versus standard hydrogen electrode (SHE) between different scenarios (*i.e.,* flow-through CDI operated in forward flow mode, flow-through CDI operated in reverse flow mode, flow-by CDI). Experimental conditions: 900 s charging at a constant potential of 1.2 V and 900 s discharging by short-circulating the two electrodes.

3.5. *Environmental implications*

Flow-through configurations have been widely applied in a number of fields including microbial fuel cells [15,16], electrochemical advanced oxidation processes [10,11], electrochemical disinfection [13,14] and capacitive desalination [9,17]. It has been reported that the fluid flow through the carbon electrode enhanced the mass transfer and promoted direct electron transfer, resulting in an increase of electrochemical kinetics and efficiencies by up to 10-fold [38,39]. Additionally, flow-through architecture provides the possibility of full utilization of the active sites of the carbon electrodes.

With regard to desalination, our results demonstrate that using a flow-through design could improve the desalination performance, a finding in line with previous work [9]. Scope exists for enhancement of the desalination performance using this promising configuration and further work should be undertaken in terms of novel electrode design, operational parameter optimization and fluid modelling.

It should be noted however that the flow-through CDI configuration promotes redox reactions to a greater extent compared to flow-by. This can be a double-edged sword. On one hand, more severe Faradaic reactions can exacerbate the oxidation of the carbon electrodes leading to desalination performance decline and energy loss. In line with more facile redox reactions, larger pH fluctuations were observed in flow-through configuration, potentially leading to more severe precipitation and scaling of the carbon electrodes with these processes reducing the long-term stability of membrane and electrode materials [40,41] In addition, these pH variations can also result in a deterioration in water quality as a result of pH values outside the accepted range. Fortunately, a number of strategies including optimization of the voltage window, constant current operation, periodic electrode polarity reversal, and use of a deoxygenation cell can be applied to effectively reduce (or even eliminate) these Faradaic side effects [21].

On the other hand, if managed properly, some of the Faradaic reactions can be beneficially utilized. For example, the H_2O_2 produced via cathodic oxygen reduction, when combined with O_3 or UV irradiation, could be potentially applied for water disinfection or contaminant degradation. In forward flow mode, the oxygen reduction reactions were enhanced with a maximum 45 μM H_2O_2 produced. As previous works have shown, this H_2O_2 concentration, if incorporated with O_3 or UV, is sufficient to promote bacterial inactivation by 0.5–2.0 log units [42–45]. In addition, if the cathode contains elemental iron or an iron oxide, the presence of electrochemically generated H_2O_2 may initiate a Fenton process with associated *in situ* generation in the CDI cell of powerful oxidants such as the hydroxyl radical which may contribute to both the degradation of any micro-pollutants present and prevention of biofilm growth on the cathode.

4. Conclusions

In this study, we have investigated both the desalination and Faradaic processes occurring in a flow-through CDI system operated in different flow modes. A flow-through CDI operated in forward flow mode exhibited the best salt removal performance compared to flow-through CDI operated in reverse flow mode and flow-by CDI. Another outcome is the recognition that pH fluctuations become more severe when adopting the flow-through configuration with the pH of the treated stream increasing to about 9.3 under forward flow mode and decreasing to 4.0 under reverse flow mode upon applying a charging voltage of 1.2 V. Additionally, the quantities of H_2O_2 generated exhibited significant differences when applying different configurations and flow modes. Specifically, the H_2O_2 produced in the CDI was 45, 37.5, and 17.6 μM, corresponding to flow-through CDI operated in forward flow mode, flow-by CDI and flow-through CDI operated in reverse flow mode, respectively, with these differences most likely a consequence of the difference in rate and extent of the occurrence of Faradaic reactions in different flow modes. Since much higher H_2O_2 concentrations are generated in forward flow mode compared to the other operational modes, this operational mode combined with O_3 or UV irradiation could potentially contribute to water disinfection or contaminant degradation during desalination.

Acknowledgement

We gratefully acknowledge funding support from the Australian Research Council through ARC Linkage Grant LP150100854. Support for Dr Jinxing Ma through a University of New South Wales (UNSW) Vice Chancellor's Postdoctoral Fellowship is gratefully acknowledged.

Appendix A. Supplementary data

Supplementary data to this article can be found online at https://doi.org/10.1016/j.electacta.2019.01.058.

References

[1] S. Porada, R. Zhao, A. van der Wal, V. Presser, P.M. Biesheuvel, Review on the science and technology of water desalination by capacitive deionization, Prog. Mater. Sci. 58 (2013) 1388–1442.

[2] M.E. Suss, S. Porada, X. Sun, P.M. Biesheuvel, J. Yoon, V. Presser, Water desalination via capacitive deionization: what is it and what can we expect from it? Energy Environ. Sci. 8 (2015) 2296–2319.

[3] W. Tang, D. He, C. Zhang, T.D. Waite, Optimization of sulfate removal from brackish water by membrane capacitive deionization (MCDI), Water Res. 121 (2017) 302–310.

[4] Y. Bian, X. Yang, P. Liang, Y. Jiang, C. Zhang, X. Huang, Enhanced desalination performance of membrane capacitive deionization cells by packing the flow chamber with granular activated carbon, Water Res. 85 (2015) 371–376.

[5] Y. Bian, P. Liang, X. Yang, Y. Jiang, C. Zhang, X. Huang, Using activated carbon fiber separators to enhance the desalination rate of membrane capacitive deionization, Desalination 381 (2016) 95–99.

[6] S.-i. Jeon, H.-r. Park, J.-g. Yeo, S. Yang, C.H. Cho, M.H. Han, D.K. Kim, Desalination via a new membrane capacitive deionization process utilizing flow-electrodes, Energy Environ. Sci. 6 (2013) 1471–1475.

[7] W. Tang, J. Liang, D. He, J. Gong, L. Tang, Z. Liu, D. Wang, G. Zeng, Various cell architectures of capacitive deionization: recent advances and future trends, Water Res. 150 (2018) 225–251.

[8] Y. Bouhadana, E. Avraham, A. Soffer, D. Aurbach, Several basic and practical aspects related to electrochemical deionization of water, AIChE J 56 (2009) 779–789.

[9] M.E. Suss, T.F. Baumann, W.L. Bourcier, C.M. Spadaccini, K.A. Rose, J.G. Santiago, M. Stadermann, Capacitive desalination with flow-through electrodes, Energy Environ. Sci. 5 (2012) 9511–9519.

[10] G. Gao, Q. Zhang, Z. Hao, C.D. Vecitis, Carbon nanotube membrane stack for flow-through sequential regenerative electro-Fenton, Environ. Sci. Technol. 49 (2015) 2375–2383.

[11] A.M. Zaky, B.P. Chaplin, Porous substoichiometric TiO_2 anodes as reactive electrochemical membranes for water treatment, Environ. Sci. Technol. 47 (2013) 6554–6563.

[12] J. Zheng, Z. Wang, J. Ma, S. Xu, Z. Wu, Development of an electrochemical ceramic membrane filtration system for efficient contaminant removal from waters, Environ. Sci. Technol. 52 (2018) 4117–4126.

[13] M.S. Rahaman, C.D. Vecitis, M. Elimelech, Electrochemical carbon-nanotube filter performance toward virus removal and inactivation in the presence of natural organic matter, Environ. Sci. Technol. 46 (2012) 1556–1564.

[14] C.D. Vecitis, M.H. Schnoor, M.S. Rahaman, J.D. Schiffman, M. Elimelech, Electrochemical multiwalled carbon nanotube filter for viral and bacterial removal and inactivation, Environ. Sci. Technol. 45 (2011) 3672–3679.

[15] K. Katuri, M.L. Ferrer, M.C. Gutiérrez, R. Jiménez, F. del Monte, D. Leech, Three-dimensional microchanelled electrodes in flow-through configuration for bioanode formation and current generation, Energy Environ. Sci. 4 (2011) 4201–4210.

[16] C. Zhang, P. Liang, Y. Jiang, X. Huang, Enhanced power generation of microbial fuel cell using manganese dioxide-coated anode in flow-through mode, J. Power Sources 273 (2015) 580–583.

[17] M. Andelman, Flow through capacitor basics, Separ. Purif. Technol. 80 (2011) 262–269.

[18] A.W. Johnson, A.W. Venolia, R.G. Wilbourne, J. Newman, C.W. Wong, W.S. Gilliam, S. Johnson, R.H. Horowitz, U. S. Dept. of the Interior, Washington, 1970..

[19] A. Johnson, J. Newman, Desalting by means of porous carbon electrodes, J. Electrochem. Soc. 118 (1971) 510–517.

[20] G. Wang, B. Qian, Y. Wang, Q. Dong, F. Zhan, J. Qiu, Electrospun porous hierarchical carbon nanofibers with tailored structures for supercapacitors and capacitive deionization, New J. Chem. 40 (2016) 3786–3792.

[21] C. Zhang, D. He, J. Ma, W. Tang, T.D. Waite, Faradaic reactions in capacitive deionization (CDI) - problems and possibilities: a review, Water Res. 128 (2018) 314–330.

[22] D. He, C.E. Wong, W. Tang, P. Kovalsky, T.D. Waite, Faradaic reactions in water desalination by batch-mode capacitive deionization, Environ. Sci. Technol. Lett. 3 (2016) 222–226.

[23] J.-H. Choi, Determination of the electrode potential causing Faradaic reactions in membrane capacitive deionization, Desalination 347 (2014) 224–229.

[24] I. Cohen, E. Avraham, Y. Bouhadana, A. Soffer, D. Aurbach, Long term stability of capacitive de-ionization processes for water desalination: the challenge of positive electrodes corrosion, Electrochim. Acta 106 (2013) 91–100.

[25] J.-H. Lee, W.-S. Bae, J.-H. Choi, Electrode reactions and adsorption/desorption performance related to the applied potential in a capacitive deionization process, Desalination 258 (2010) 159–163.

[26] E. Avraham, M. Noked, I. Cohen, A. Soffer, D. Aurbach, The dependence of the desalination performance in capacitive deionization processes on the electrodes PZC, J. Electrochem. Soc. 158 (2011) 168–173.

[27] E.M. Remillard, A.N. Shocron, J. Rahill, M.E. Suss, C.D. Vecitis, A direct comparison of flow-by and flow-through capacitive deionization, Desalination 4444 (2018) 169–177.

[28] Y.S. Dzyazko, A. Rudenko, Y.M. Yukhin, A. Palchik, V. Belyakov, Modification of ceramic membranes with inorganic sorbents. Application to electrodialytic recovery of Cr (VI) anions from multicomponent solution, Desalination 342 (2014) 52–60.

[29] M. Asraf-Snir, J. Gilron, Y. Oren, Scaling of cation exchange membranes by gypsum during Donnan exchange and electrodialysis, J. Membr. Sci. 567 (2018) 28–38.

[30] W. Tang, D. He, C. Zhang, P. Kovalsky, T.D. Waite, Comparison of Faradaic reactions in capacitive deionization (CDI) and membrane capacitive deionization (MCDI) water treatment processes, Water Res. 120 (2017) 229–237.

[31] C. Zhang, J. Ma, D. He, T.D. Waite, Capacitive membrane stripping for ammonia recovery (CapAmm) from dilute wastewaters, Environ. Sci. Technol. Lett. 5 (2017) 43–49.

[32] C. Zhang, J. Ma, J. Song, C. He, T.D. Waite, Continuous ammonia recovery from wastewaters using an integrated capacitive flow electrode membrane stripping system, Environ. Sci. Technol. (2018), https://doi.org/10.1021/acs.est.8b02743.

[33] C. He, J. Ma, C. Zhang, J. Song, T.D. Waite, Short-circuited closed-cycle operation of flow-electrode CDI for brackish water softening, Environ. Sci. Technol. (2018) 9350–9360.

[34] J. Ma, D. He, W. Tang, P. Kovalsky, C. He, C. Zhang, T.D. Waite, Development of redox-active flow electrodes for high-performance capacitive deionization, Environ. Sci. Technol. 50 (2016) 13495–13501.

[35] C. Zhang, D. He, J. Ma, T.D. Waite, Active chlorine mediated ammonia oxidation revisited: reaction mechanism, kinetic modelling and implications, Water Res. 145 (2018) 220–230.

[36] D. He, J. Ma, R.N. Collins, T.D. Waite, Effect of structural transformation of nanoparticulate zero-valent iron on generation of reactive oxygen species, Environ. Sci. Technol. 50 (2016) 3820–3828.

[37] Y. Zhou, Q. Ji, H. Liu, J. Qu, Pore structure-dependent mass transport in flow-through electrodes for water remediation, Environ. Sci. Technol. (2018) 7477–7485.

[38] H. Liu, A. Vajpayee, C.D. Vecitis, Bismuth-doped tin oxide-coated carbon nanotube network: improved anode stability and efficiency for flow-through organic electrooxidation, ACS Appl. Mater. Interfaces 5 (2013) 10054–10066.

[39] Q. Ji, D. Yu, G. Zhang, H. Lan, H. Liu, J. Qu, Microfluidic flow through polyaniline supported by lamellar-structured graphene for mass-transfer-enhanced electrocatalytic reduction of hexavalent chromium, Environ. Sci. Technol. 49

(2015) 13534–13541.

[40] O. Nir, N.F. Bishop, O. Lahav, V. Freger, Modeling pH variation in reverse osmosis, Water Res. 87 (2015) 328–335.

[41] I. Cohen, E. Avraham, Y. Bouhadana, A. Soffer, D. Aurbach, The effect of the flow-regime, reversal of polarization, and oxygen on the long term stability in capacitive de-ionization processes, Electrochim. Acta 153 (2015) 106–114.

[42] M. Cho, V. Gandhi, T.M. Hwang, S. Lee, J.H. Kim, Investigating synergism during sequential inactivation of MS-2 phage and Bacillus subtilis spores with UV/H_2O_2 followed by free chlorine, Water Res. 45 (2011) 1063–1070.

[43] M. Cho, J. Yoon, Enhanced bactericidal effect of O_3/H_2O_2 followed by Cl_2, Ozone: Sci. Eng. 28 (2006) 335–340.

[44] M. Lanao, M. Ormad, C. Ibarz, N. Miguel, J. Ovelleiro, Bactericidal effectiveness of O3, O_3/H_2O_2 and O_3/TiO_2 on clostridium perfringens, Ozone: Sci. Eng. 30 (2008) 431–438.

[45] D. Rubio, E. Nebot, J.F. Casanueva, C. Pulgarin, Comparative effect of simulated solar light, UV, UV/H_2O_2 and photo-Fenton treatment (UV-Vis/H_2O_2/$Fe^{2+,3+}$) in the Escherichia coli inactivation in artificial seawater, Water Res. 47 (2013) 6367–6379.